



The modelling of anchors using the material point method

C. J. Coetzee^{1,*}, P. A. Vermeer² and A. H. Basson¹

¹*Department of Mechanical Engineering, University of Stellenbosch, South Africa*

²*Institut für Geotechnik, Universität Stuttgart, Germany*

SUMMARY

The ultimate capacity of anchors is determined using the material point method (MPM). MPM is a so-called meshless method capable of modelling large displacements, deformations and contact between different bodies. A short introduction to MPM is given and the derivation of the discrete governing equations. The analysis of a vertically loaded anchor and one loaded at 45° is presented. The load–displacement curves are compared to that obtained from experiments and the effect of soil stiffness and anchor roughness is investigated. The results of the vertically loaded anchor are also compared to an analytical solution. The displacement of the soil surface above the anchor was measured and compared to the numerical predictions. Convergence with mesh refinement is demonstrated and the effect of mesh size and dilatancy angle on the shear band width and orientation is indicated.

The results show that MPM can model anchor pull out successfully. No special interface elements are needed to model the anchor–soil interface and the predicted ultimate capacities were within 10% of the measured values. Copyright © 2005 John Wiley & Sons, Ltd.

KEY WORDS: material point method; anchor pull out

1. INTRODUCTION

In many engineering problems, such as silo discharging and earthmoving processes, large displacements and deformations occur. When these problems are modelled with a Lagrangian finite element method, the mesh becomes so distorted that re-meshing is needed. During the re-meshing process all the state variables have to be mapped from the distorted mesh to the newly defined mesh, which introduces errors [1].

Large deformation problems can, however, be solved using so-called meshless methods. These methods trace the history of the state variables at material points, which are not connected to the element mesh. The mesh does not deform, and the problem of severe mesh distortion is overcome. The meshless methods can be classified in four basic groups [2]: moving weighted least square approximations, kernel methods, partition of unity methods, and particle methods (particle-in-cell, material point).

*Correspondence to: C. J. Coetzee, Department of Mechanical Engineering, University of Stellenbosch, Private Bag X1, 7602 Matieland, South Africa.

†E-mail: ccoetzee@sun.ac.za

Received 13 January 2004

Revised 20 January 2005

Accepted 16 February 2005

1 A particle-in-cell method (PIC) was first used to model fluid dynamics by Harlow [3].
 2 A variation of the method has been successfully applied to solid mechanics by Burgess *et al.* [4],
 3 Sulsky *et al.* [5, 6] and Sulsky and Schreyer [7, 8]. They called it the material point method
 4 (MPM), and showed the capability of MPM to model problems such as impact and penetration.
 5 MPM can be classified as a finite element method formulated in an arbitrary Lagrangian–
 6 Eulerian description of motion. State variables are traced at material points. The Eulerian mesh
 7 is defined independently from the material points. The equations of motion are formulated and
 8 solved on the mesh. Since all state variables are traced at the material points, the mesh can be
 9 defined in an arbitrary way and the problem of mesh distortion is avoided.

10 This paper briefly describes the theory behind MPM and derives the discrete governing
 11 equations. The pull out of anchors is modelled to demonstrate the ability of MPM to model
 12 geotechnical processes associated with relatively large displacements and deformations. It is also
 13 shown that the frictional contact between the anchor and the sand can be modelled using a
 14 special contact algorithm, but without the use of special interface elements.

15 Anchors form an important component of many civil engineering projects. Anchors are
 16 typically used to support other structures such as towers, bridges and roofs. Rowe and Davis
 17 [9, 10] review the methods used to model and analyse anchor behaviour. The prediction of
 18 anchor plate behaviour is usually restricted to the limiting conditions of elastic displacement or
 19 ultimate capacity. The elastic analysis only yields a load–displacement response within the
 20 elastic range. Many approaches have been given to estimate the ultimate capacity or collapse
 21 load. These methods involve the use of limit equilibrium concepts, the method of characteristics
 22 and empirical corrections. In general, anchor behaviour is influenced by the material properties,
 23 the initial stress state, the boundary conditions and the anchor roughness [10].

24 As validation, the passive resistance of rectangular anchors embedded in sand is modelled.
 25 The results are compared to experimental results, under the assumption of plane strain.
 26 Vertically pulled anchors and anchors pulled upwards at an angle of 45° are investigated.
 27
 28

31 2. THE MATERIAL POINT METHOD

32 In the first part of this section, index notation is used to denote vectors and matrices. The
 33 subscripts i, j and k are used, assuming values of 1, 2 and 3, unless stated otherwise. In the latter
 34 part of the section, Hassenpflug [11] notation is used. A column vector is indicated by a *overbar*,
 35 $\bar{\mathbf{x}}$, a row vector by a *underbar*, $\underline{\mathbf{x}}$ and a matrix by both, $\underline{\underline{\mathbf{x}}}$. Plane strain conditions are assumed.
 36
 37

39 2.1. Space discretization

40 First, the initial configuration of the body is divided into a number of subregions. This is done as
 41 depicted in Figure 1. In the centre of each subregion a material point or particle is placed. This
 42 material point represents the subspace, and is given a mass m_p . The mass is calculated by
 43 assuming that the whole mass of the subregion is concentrated at the material point. The mass
 44 of a material point is constant and does not change with time or position. The density $\rho(x_i)$
 45 represented by this collection of discrete mass points is approximated using the Dirac delta
 function

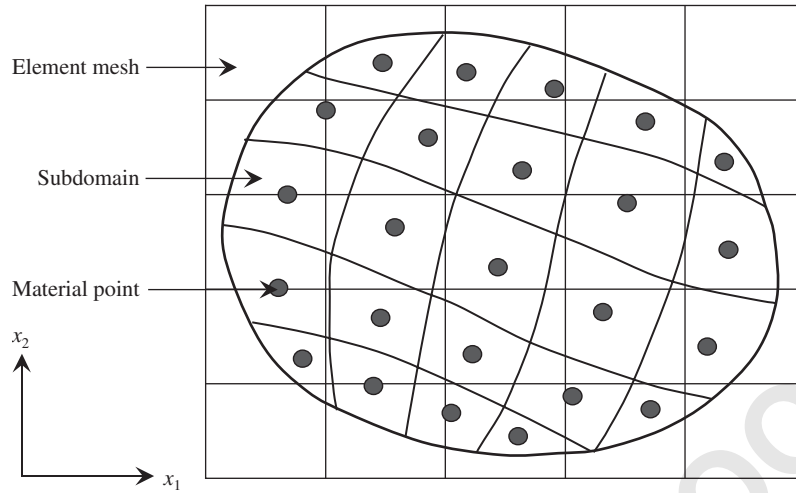


Figure 1. The element mesh and material points (particles) within the subdomains.

$$\rho(x_i) = \sum_{p=1}^{N_p} m_p \delta(x_i - x_i^p) \quad (1)$$

where x_i is an arbitrary position vector, x_i^p is the position vector at material point p , N_p is the total number of material points and the Dirac delta function is defined as follows:

$$\delta(x - a) = \begin{cases} 0 & x \neq a \\ \infty & x = a \end{cases} \quad \text{and} \quad \int_{-\infty}^{+\infty} \delta(x - a) dx = 1 \quad (2)$$

For clarity, the equations of motion are derived for a single element only. The whole system would be analysed by assembling the matrices and vectors as in standard FEM routines. The mass of each material point is fixed which ensures mass conservation.

The weak form of the linear momentum equation is given by

$$\int_V \rho \frac{dv_i}{dt} w_i dV = \int_V \rho f_i w_i dV - \int_V \rho \sigma_{ij}^s w_{i,j} dV + \int_S \tau_i w_i dS \quad (3)$$

where v_i is the velocity vector, f_i the body forces and τ_i the surface traction acting on surface S and w_i is test function. σ_{ij}^s is the specific stress tensor defined as the Cauchy stress tensor divided by the material density. Substitution of the discrete density representation, Equation (1), into Equation (3) and making use of the definition of the Dirac delta function yields a discrete expression where the integration is performed as a sum of material point properties.

$$\sum_{p=1}^{N_p} m_p \frac{dv_i^p}{dt} w_i^p = \sum_{p=1}^{N_p} m_p f_i^p w_i^p - \sum_{p=1}^{N_p} m_p \sigma_{ij}^{sp} w_{i,j}^p + \int_S \tau_i w_i dS \quad (4)$$

The superscript p indicates a variable evaluated at the material point. For example, the specific stress $\sigma_{ij}^{sp} \equiv \sigma_{ij}^p(x_i^p)$.

1 *2.2. Element formulation*

3 The element mesh used is similar to that of FEM. Four noded quadrilateral elements are used.
 4 Under the assumption of two-dimensional conditions, the acceleration field $\dot{v}_i \equiv dv_i/dt$, for
 5 example, can be written in terms of nodal and shape function values

$$\dot{\mathbf{v}}(\mathbf{x}, t) \equiv [\dot{v}_1 \ \dot{v}_2]^T = \underline{\mathbf{N}} \dot{\mathbf{v}}^n \quad (5)$$

7 where $\underline{\mathbf{N}}$ is a matrix containing the shape functions. The element nodal acceleration vector, $\dot{\mathbf{v}}^n$,
 8 contains the nodal values of the acceleration field. The same can be applied to the vector field w_i
 9 to obtain a vector $\bar{\mathbf{w}}$. Define the following vectors under plane strain conditions:

$$\bar{\sigma}^s \equiv \begin{bmatrix} \sigma_{11}^s \\ \sigma_{22}^s \\ \sigma_{12}^s \end{bmatrix}, \quad \bar{\mathbf{f}} \equiv \begin{bmatrix} f_1 \\ f_2 \end{bmatrix}, \quad \bar{\tau} \equiv \begin{bmatrix} \tau_1 \\ \tau_2 \end{bmatrix} \quad (6)$$

11 with $\sigma_{12}^s = \sigma_{21}^s$. Note that under the assumption of plane strain, the third normal stress
 12 component σ_{33}^s is not included in the definition above. This component is, however, calculated at
 13 each material point and used in the constitutive model. Using these definitions, Equation (4) can
 14 be written as follows:

$$\bar{\mathbf{w}}^T \sum_{p=1}^{N_p} m_p (\underline{\mathbf{N}}^p)^T \underline{\mathbf{N}}^p \dot{\mathbf{v}}^n = \bar{\mathbf{w}}^T \sum_{p=1}^{N_p} m_p (\underline{\mathbf{N}}^p)^T \bar{\mathbf{f}}^p - \bar{\mathbf{w}}^T \sum_{p=1}^{N_p} m_p (\underline{\mathbf{B}}^p)^T \bar{\sigma}^{sp} + \bar{\mathbf{w}}^T \int_S (\underline{\mathbf{N}}^p)^T \bar{\tau} \, dS \quad (7)$$

15 where the superscript p indicates values to be evaluated at the material points, e.g. $\underline{\mathbf{N}}^p \equiv \underline{\mathbf{N}}(\mathbf{x}^p)$.
 16 The arbitrary test vector $\bar{\mathbf{w}}$ appears in all the above terms and can thus be dropped. The final
 17 discretized system of equations follows as

$$\underline{\mathbf{M}} \dot{\mathbf{v}}^n = \bar{\mathbf{F}}^{\text{int}} + \bar{\mathbf{F}}^{\text{ext}} \quad (8)$$

19 where the *mass matrix* $\underline{\mathbf{M}}$ is given by

$$M_{ij} \equiv \underline{\mathbf{M}} = \sum_{p=1}^{N_p} m_p (\underline{\mathbf{N}}^p)^T \underline{\mathbf{N}}^p \quad (9)$$

21 the *internal-force vector* is given by

$$F_i^{\text{int}} \equiv \bar{\mathbf{F}}^{\text{int}} = - \sum_{p=1}^{N_p} m_p (\underline{\mathbf{B}}^p)^T \bar{\sigma}^{sp} \quad (10)$$

23 and the *external-force vector* is given by

$$F_i^{\text{ext}} \equiv \bar{\mathbf{F}}^{\text{ext}} = \int_S (\underline{\mathbf{N}}^p)^T \bar{\tau} \, dS \quad (11)$$

25 The matrix $\underline{\mathbf{B}}^p$ contains shape function gradients. In practice, to simplify computations, a
 26 lumped mass matrix may be used instead of the consistent mass matrix given by Equation (9).
 27 The lumped mass matrix is a diagonal matrix with each entry being the corresponding row sum
 28 of the consistent mass matrix. Matrix inversions become trivial if a lumped matrix is used, at the
 29 cost of introducing a small amount of numerical dissipation [4, 12]. The consistent mass matrix
 30 can also be singular for certain arrangements of the particles. There appears to be only a few
 31 arrangements of particles that yield a singular consistent mass matrix, but nearby arrangements

1 might result in an ill-conditioned matrix. On the other hand, the lumped matrix is diagonal and
2 well conditioned.

3 2.3. Time integration

5 Let the time step size be Δt . The solution to the system of Equations (8) is found at discrete
7 instants in time $t, t + 1, \dots, t + n$. The calculation during each time increment consists of three
9 phases; a initialization phase, a Lagrangian phase and a convective phase [5].

11 2.3.1. *Initialization phase.* Assume that the position and velocity vector, stress tensor, strain
13 tensor and history-dependent variables of each material point are known at time t . With the
15 position of each particle known, its shape function values can be computed and hence the mass
17 matrix, $\bar{\mathbf{M}}^t$, given by Equation (9). Mapping of the particle velocities to the nodes, provides the
19 initial data for the solution to Equation (8). The following equation is solved to obtain the nodal
21 velocity $\bar{\mathbf{v}}^{n,t}$ at time t .

$$17 \quad \bar{\mathbf{M}}^t \bar{\mathbf{v}}^{n,t} = \sum_{p=1}^{N_p} m_p (\bar{\mathbf{N}}^{p,t})^T \begin{bmatrix} v_1^{p,t} \\ v_2^{p,t} \end{bmatrix} \quad (12)$$

19 where $([v_1^{p,t} \ v_2^{p,t}])^T$ is the material point velocity vector at time t , containing the velocity
21 components in the x_1 - and x_2 -directions, respectively. This equation expresses equivalence of
23 momentum calculated for the material points and for the nodes [1].

25 2.3.2. *Lagrangian phase.* With the shape functions of each particle known, the internal- and
27 external-force vectors can be calculated using Equations (10) and (11), respectively. With these
29 two vectors and the mass matrix known, Equation (8) is solved for the nodal acceleration at
31 time t .

$$27 \quad \ddot{\mathbf{v}}^{n,t} = (\bar{\mathbf{M}}^t)^{-1} (\bar{\mathbf{F}}^{\text{int},t} + \bar{\mathbf{F}}^{\text{ext},t}) \quad (13)$$

29 The ‘new’ nodal velocity, $\bar{\mathbf{v}}^{n,t+1}$, at time $t + 1$ is obtained by using an explicit time integrator

$$31 \quad \bar{\mathbf{v}}^{n,t+1} = \bar{\mathbf{v}}^{n,t} + \Delta t \ddot{\mathbf{v}}^{n,t} \quad (14)$$

33 which obviously requires very small time steps to ensure accuracy. Using the new nodal velocity,
35 the increment in strains can be calculated at the particles. Define the vector of strain increment
37 as follows

$$35 \quad \Delta \bar{\boldsymbol{\varepsilon}}^p \equiv [\varepsilon_{11}^p \quad \varepsilon_{22}^p \quad \varepsilon_{12}^p]^T \quad (15)$$

37 This vector can be calculated using matrix $\bar{\mathbf{B}}^{p,t}$

$$39 \quad \Delta \bar{\boldsymbol{\varepsilon}}^{p,t+1} = \Delta t \bar{\mathbf{B}}^{p,t} \bar{\mathbf{v}}^{n,t+1} \quad (16)$$

41 With the increment in strain known, the new stress state $\bar{\boldsymbol{\sigma}}^{p,t+1}$ at each material point can be
43 calculated based on the chosen constitutive model. One way of doing this, would be to calculate
45 the stress increment, using the tangent modulus $\bar{\mathbf{M}}^{p,t}$

$$43 \quad \Delta \bar{\boldsymbol{\sigma}}^{p,t+1} = \bar{\mathbf{M}}^{p,t} \Delta \bar{\boldsymbol{\varepsilon}}^{p,t+1} \quad (17)$$

45 The use of the tangent modulus in a numerical algorithm, however, results in a tendency for the
stress to drift from the yield surface [6]. In practice a incremental iterative scheme is rather used.
With the given increment in strain, the material is assumed to be elastic, and a trial stress state is

1 computed. The yield function f is evaluated using the trial state, and if $f \leq 0$ the material point is
 2 still in the elastic region and no further calculations are needed. However, if $f > 0$, return
 3 algorithms, based on the flow potential g , are needed to force f back to zero. In the case of a
 4 Mohr–Coulomb or Drucker–Prager model, a simple one-step return to the yield surface is
 5 possible [13]. For other models like Lade, a iterative procedure is needed.

6 History-dependent variables such as strain-hardening parameters may also be updated at this
 7 stage. During the Lagrangian phase the nodes are assumed to move at the computed nodal
 8 velocity $\bar{\mathbf{v}}^{n,t+1}$. Thus, points in the interior of the element move in proportion to the motion of
 9 the nodes, as given by the representation using the nodal shape functions. Since shape functions
 10 are used to map the nodal velocity continuously to the interior of the element, the positions of
 11 the material points are updated by moving them in a single-valued, continuous velocity field.
 12 Similarly, the velocity of a material point is updated by mapping the nodal accelerations to the
 13 material point position. The updated position vector and velocity vector follow as

$$15 \quad \bar{\mathbf{x}}^{p,t+1} = \bar{\mathbf{x}}^{p,t} + \Delta t \bar{\mathbf{N}}^{p,t} \bar{\mathbf{v}}^{n,t+1}; \quad \bar{\mathbf{v}}^{p,t+1} = \bar{\mathbf{v}}^{p,t} + \Delta t \bar{\mathbf{N}}^{p,t} \dot{\bar{\mathbf{v}}}^{n,t} \quad (18)$$

16 Because the velocity field is single-valued, interpenetration of material is precluded. This feature
 17 of the algorithm allows simulations of impact and penetration without the need for a special
 18 contact algorithm.

19 **2.3.3. Convective phase.** At this point in the computational cycle, the material points are
 20 completely updated and carry the complete solution, i.e. all the state variables needed to start a
 21 new calculation step are carried by the material points. During the convective phase, the
 22 material points are held fixed and the element mesh can be redefined. The mesh can be chosen in
 23 any convenient manner, for example adaptive meshes can be used to resolve sharp gradients and
 24 interfaces. The simplest and most convenient choice is, however, to keep the existing mesh. Any
 25 motion of the mesh relative to the material points model convection. Since the material points
 26 do not move during the convective phase, material point properties have the same value at the
 27 end of the convective phase as they had at the end of the Lagrangian phase. This completes the
 28 computational cycle. A new cycle is begun using the information carried by the material points
 29 to initialize nodal values on the element mesh.

31 2.4. Stability

32 In the previous sections, a simple explicit time integrator is used of which the time step should
 33 satisfy the stability condition, i.e. the critical time step should be the smallest ratio of the element
 34 size to the wave speed through the material. For small displacements, the spatial discretization
 35 in MPM is equivalent to that of FEM using Gauss points at the same locations as those of the
 36 material points in each element. Therefore, the convergence behaviour of the integrator used is
 37 similar to that employed to integrate the corresponding equations in FEM. However, according
 38 to Chen *et al.* [14], no consistent theoretical results have been obtained for the convergence
 39 behaviour of time integrators when larger deformations occur and a reasonable time step is
 40 usually found through numerical experiments.

43 2.5. Contact model

44 The MPM formulation presented here automatically enforces no-slip contact between two
 45 different bodies. The reason for this is that a single-valued velocity field is used for updating the

particle positions. Bardenhagen *et al.* [15], however, developed an algorithm which relaxes the no-slip condition and allows Coulomb friction and slip at contacting boundary nodes. This contact algorithm was implemented to model the anchor–soil interface. The theory behind the contact model is not presented here and the reader is referred to Reference [15].

3. VERTICALLY PULLED ANCHOR

Rowe and Davis [9] investigated the behaviour of vertically and horizontally pulled anchors in sand. Model tests were performed using a dry, medium grained quartz Sydney sand. The tests were performed in a steel box $450 \text{ mm} \times 606 \text{ mm} \times 692 \text{ mm}$ high, Figure 2. The anchor was a 51 mm wide and 8 mm thick mild steel plate with length to breadth ratios of $L/B = 1, 2, 3, 4, 5, 8.75$. All of the experimental load–displacement curves were not published, and only the results with a ratio of $L/B = 8.75$ are used for comparisons. The load was applied to the centre of the anchor via a 8 mm diameter rod at a constant velocity of 0.025 mm s^{-1} .

The anchor plate was put on top of a 140 mm layer of sand in the bottom of the box. Additional sand was then added until the anchor was buried to the required depth. The sand was sprinkled from a height of 25 mm above the surface. The unit weight of the sand γ was determined by weighing the sand in the box and measuring the total volume occupied. Triaxial tests were performed to determine the friction and dilatancy angles. No attempt was made to measure the coefficient at rest (K_0), of the sand in the box, but empirical correlations were used to make an estimate [9]. Poisson's ratio was also estimated. The stiffness of the material was not measured, and simulations were performed with different stiffness values.

Figure 3 shows the simulation model. A symmetry plane was used to model only half of the problem depicted in Figure 2. The other boundary conditions are shown in the figure. Initial stresses were specified using $K_0 = 0.47$. Damping [13] was used to reach an equilibrium state,

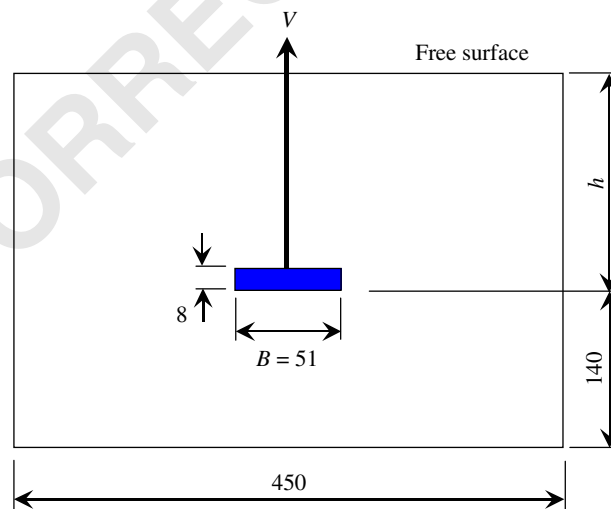
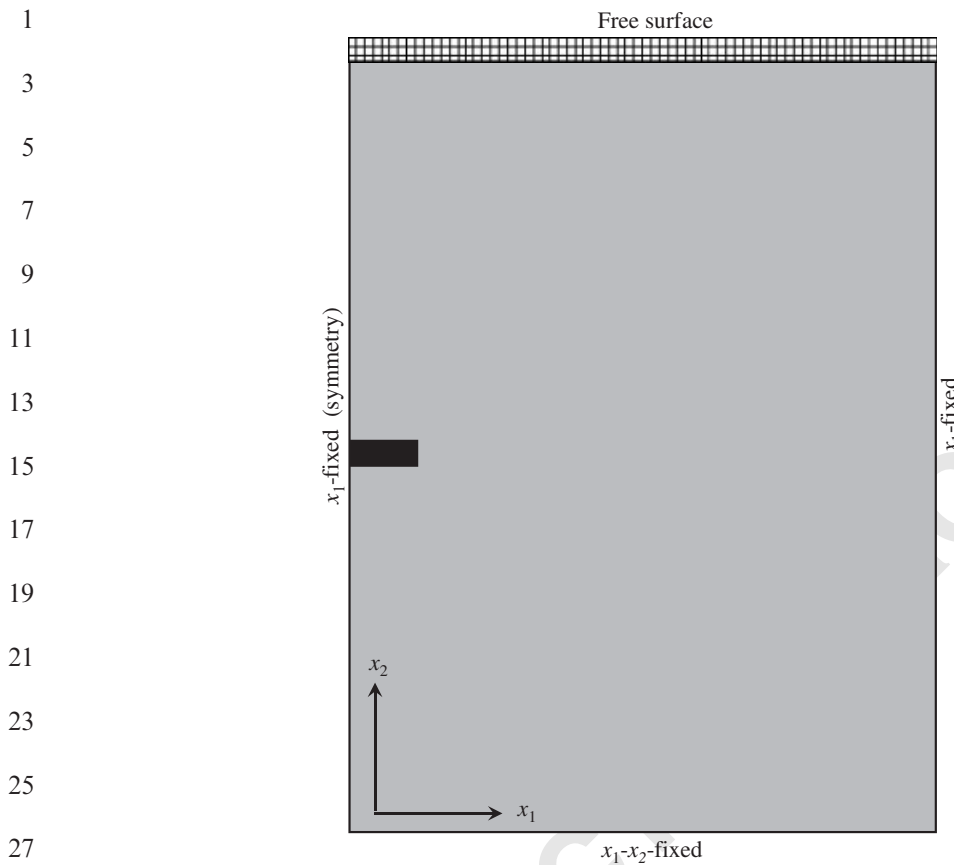


Figure 2. Geometry for vertically pulled anchor. Dimensions are in mm.



29 Figure 3. Simulation model for vertically pulled anchor.

31
33 Table I. Mohr–Coulomb material data for the vertical anchor pull out.

Description	Symbol	Value
Young's modulus	E	700/1000 MPa
Poisson's ratio	ν	0.2
Unit weight	γ	14.9 kN m ⁻³
Friction angle	ϕ	32°
Dilatancy angle	ψ	4°
Cohesion	c	0 Pa
Material–wall friction	μ_{wall}	Smooth/rough
Coefficient of earth pressure	K_0	$1 - \sin(\phi) = 0.47$

35
37
39
41
43
45 after which the damping was removed and the anchor, modelled as a rigid body, moved at constant velocity in the x_2 -direction (vertical). The material properties are summarized in Table I. Soil behaves highly non-linear which makes it difficult to predict the pre-failure

behaviour using a bilinear Mohr–Coulomb model. However, when interested in the ultimate capacity (failure load), the Mohr–Coulomb model is reasonably accurate at fully developed plastic flow. It is assumed that the complex pre-failure soil behaviour does not influence the ultimate capacity. This is verified by showing that different values for Young’s modulus does not influence the ultimate capacity.

Two embedded ratios were used for comparison: $h/B = 3$ and $h/B = 5$. The domain was divided into 44×58 and 44×78 square elements, respectively, to model the different ratios. Figure 4 shows the load–displacement curves for $h/B = 3$, stiffness values of $E = 700$ MPa and $E = 1000$ MPa and a rough and smooth sand–anchor interface. The higher stiffness value of $E = 1000$ MPa clearly follows the experimental result more closely in the initial elastic region. The difference between a rough and smooth interface has no significant effect on the ultimate capacity, which is within 5% of the measured value. It is also observed by Rowe and Davis [9] that for vertically pulled anchors, the anchor roughness has little effect on the ultimate capacity.

Figure 5 shows the experimental and numerical results for $h/B = 5$. The anchor is assumed to be smooth and the stiffness taken as $E = 1000$ MPa. The simulation accurately predicts the load–displacement behaviour in the elastic region and over predicts the ultimate capacity by roughly 3%.

All of the above simulations were performed using a Mohr–Coulomb constitutive model with the parameters given in Table I. Figure 6 shows the results using a Drucker–Prager model. The same friction and dilatancy angles were used, and the Drucker–Prager parameters were chosen

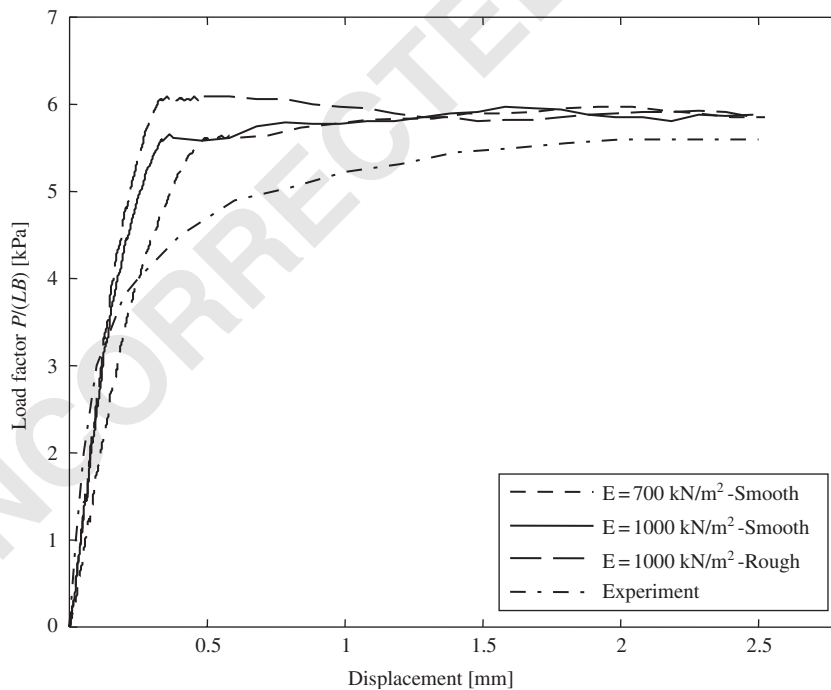


Figure 4. Load–displacement curve for vertically pulled anchor, $h/B = 3$.

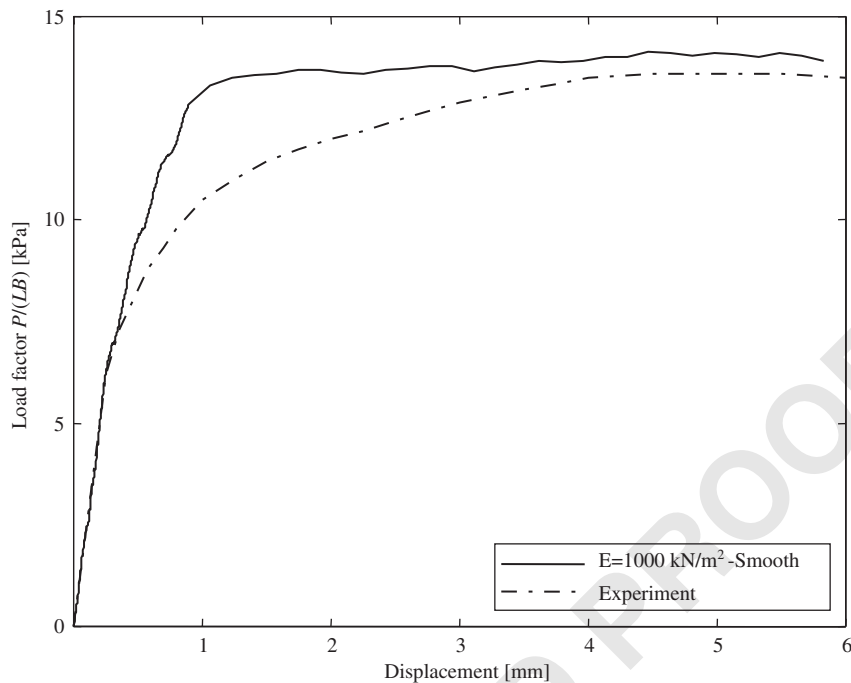


Figure 5. Load–displacement curve for vertically pulled anchor, $h/B = 5$.

such that the yield surface fits within the Mohr–Coulomb yield surface (inner adjustment [13]). Using the Drucker–Prager model, there is a slightly more gradual transition from the elastic state to the plastic state. The ultimate capacity, however, is the same. The experiments were all three-dimensional, while the simulations were two-dimensional. The effect of the edges of the anchor might be the reason for the differences in measured and calculated loads.

Vermeer and Sutjiadi [16] derived an analytical expression for the ultimate load factor of vertically loaded anchors with $L \gg B$. It is shown that,

$$\frac{P}{\gamma BLh} = 1 + \frac{h}{B} \tan \alpha \quad (19)$$

with

$$\tan \alpha = \frac{\sin \phi \cos \psi}{1 - \sin \phi \sin \psi} \quad (20)$$

Using this expression with $h/B = 3$, the load factor $P/LB = 6.03$ kPa and with $h/B = 5$, the load factor $P/LB = 14.23$ kPa. There is a very good agreement with the results in Figures 4 and 5, respectively.

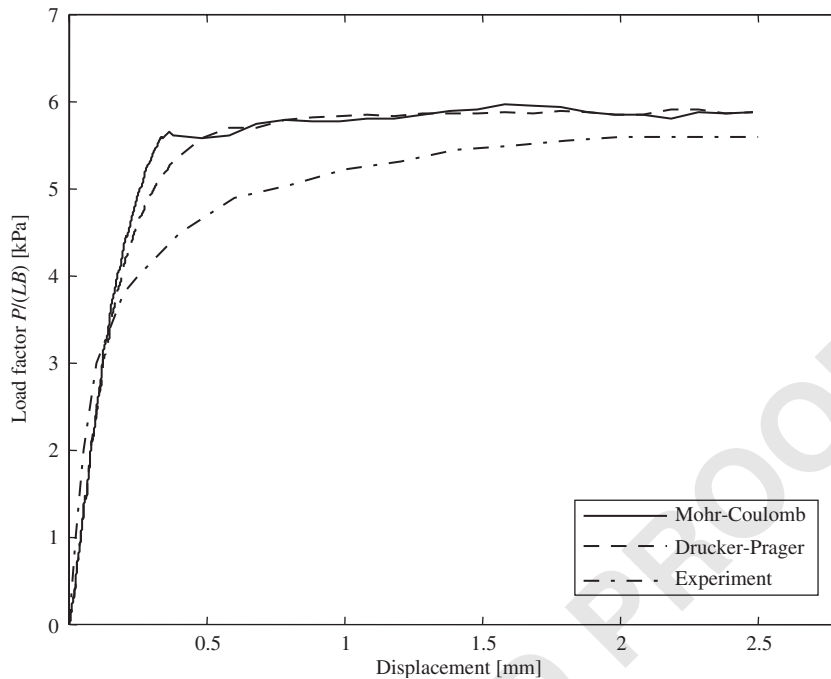


Figure 6. Comparison between Mohr–Coulomb and Drucker–Prager models on vertically pulled anchor, $h/B = 3$, smooth interface, $E = 1000$ MPa.

4. ANCHOR PULLED AT 45°

Murray and Geddes [17] experimentally investigated the behaviour of anchors pulled at angles of 0–90° with the vertical. In this analysis, comparisons are made only to the case where the anchor was pulled at 45°. The results are also compared to that of upper and lower bound analysis where the limit theorems of soil plasticity have been used. The upper and lower bound theorems enable the theoretical failure load of an idealized material to be bracketed. These theorems are based on the Mohr–Coulomb constitutive model [17]. Figure 7 shows the problem geometry. The anchor width $B = 51$ mm is the same as in the previous section, but the thickness $t = 6.35$ mm differs. The anchor width to length ratio used for comparisons is $L/B = 10$, although experiments were also performed for ratios $L/B = 1, 2$ and 5.

A medium grained sand, known as Portishead Fines, was compacted in layers by vibration with the anchor fixed in position in the test container. The sand in the container was weighed to calculate the average unit weight γ . Direct shear box tests on the sand yielded the friction angle ϕ and cohesion c . A modified shear box was used to determine the interface friction μ_{wall} . No attempt has been made to determine the material stiffness E , Poisson's ratio ν , the dilatancy angle ψ or the coefficient at rest K_0 . It has, however, been shown in the previous section that the stiffness has little effect on the limit load. Poisson's ratio is taken to be $\nu = 0.2$ and Murray and Geddes [17] estimated the dilatancy angle to be within the range $\psi = 5\text{--}12^\circ$. Table II summarizes

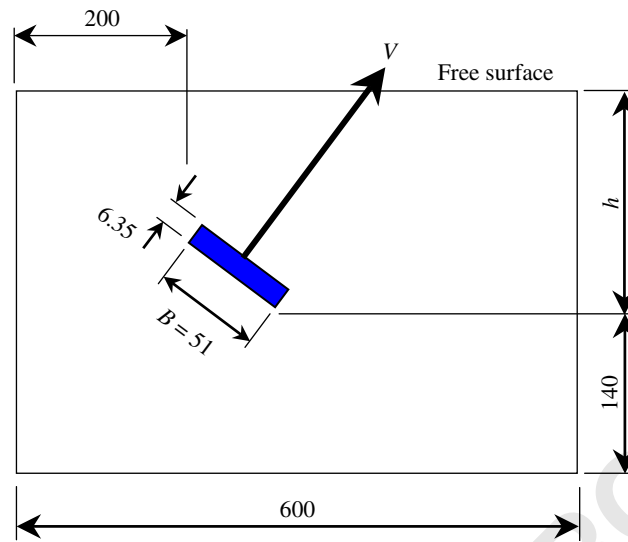


Figure 7. Geometry for anchor pulled at 45° . Dimensions are in mm.

Table II. Mohr–Coulomb material data for 45 anchor pull out.

Description	Symbol	Value
Young's modulus	E	1500 MPa
Poisson's ratio	ν	0.2
Unit weight	γ	16.8 kN m^{-3}
Friction angle	ϕ	44°
Dilatancy angle	ψ	12°
Cohesion	c	0 Pa
Anchor–sand friction	μ_{wall}	11° (0.19)
Coefficient of earth pressure	K_0	$1 - \sin(\phi) = 0.31$

the material properties used. A symmetry plane could not be used as in the previous example and the domain was divided into 80×32 , 80×45 and 80×59 square elements for the different embedded ratios $h/B = 2, 4$ and 6 .

Murray and Geddes [17] do not provide the load–displacement curves obtained from their experiments, but only give the ultimate loads for different embedded depths. The definition given by Rowe and Davis [9, 10] is used to determine the ultimate capacity, given a load–displacement curve. The k_n failure load is defined as the load which produces n times the displacement that would have occurred had the soil remained elastic. This definition is not dependent on scale or stiffness modulus, but the value of n remains arbitrary. Rowe and Davis [9, 10] suggest a value $n = 4$, i.e. a k_4 failure load. Figure 8 plots the dimensionless load factor

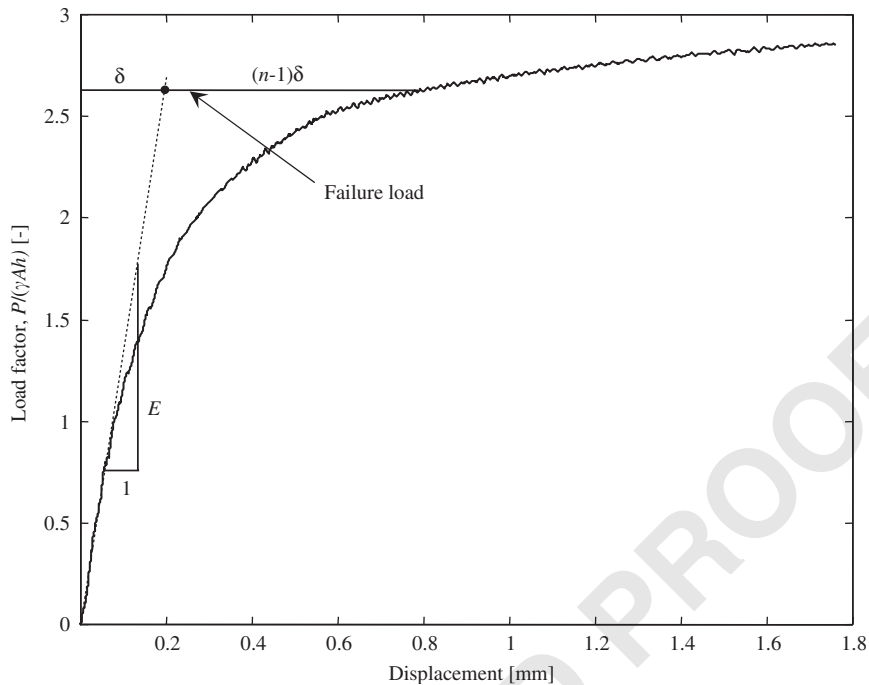


Figure 8. Load–displacement curve for anchor pulled at 45, $h/B = 2$.

$P/\gamma Ah$ against the anchor displacement. P is the load on the anchor measured in N , γ the unit weight, $A = BL$ is the frontal area of the anchor and h the embedded depth. The calculation of the k_n failure load is also shown by the figure.

The ultimate failure loads at different depth ratios are plotted in Figure 9. The simulations under predict the measured ultimate capacity for all three depth ratios. The maximum difference is 9.3%. The upper-bound limit is also shown. The biggest unknown in this problem is the initial stress state. The value of K_0 has been taken to be $1 - \sin(\phi)$ according to Jaky [18]. The way of preparing the sand bed, however, will have an influence on this value. Rowe and Davis [9] have shown, that for a particular case, an increase in K_0 from 0.5 to 1.0, caused a 6% increase in the ultimate capacity.

Murray and Geddes [17] measured the vertical movement of the free surface directly above the anchor. The numerical results are compared to the measured movements in Figure 10 at anchor displacements of 0.35, 0.70, 1.00 and 1.43 mm. The predictions are accurate within 12.5% of the maximum measured movement. The MPM velocity field is also shown at a anchor displacement of 1.43 mm. The upper bound method predicts a larger volume of material failing, as indicated by the two slip lines. The upper bound method, however, assumes an associated flow rule ($\psi = \phi$) which might be the reason for predicting a larger failure region.

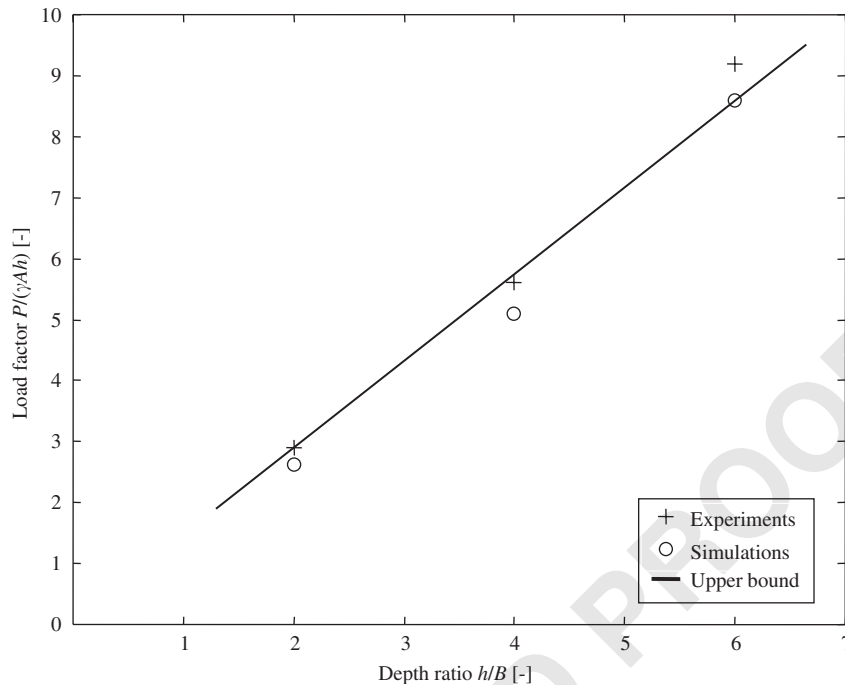


Figure 9. The ultimate capacity at different depth ratios for the anchor pulled at 45.

5. CONVERGENCE AND SHEAR ZONES

The vertically pulled anchor is used to demonstrate convergence with mesh refinement. Figure 11 shows the load–displacement curves using three mesh sizes: 25×32 , 32×42 and 44×58 . It is clear that with a refinement in mesh size, the ultimate capacity converges to the experimental value.

In Figure 12 the shear strain intensity is used to show the computed shear bands for different mesh sizes. With a refinement in mesh size, the shear band decreases slightly in width. Vermeer and Sutjiadi [16] shows that the angle of the shear band with the vertical is equal to the dilatancy angle. The shear band stretches from the anchor edge vertically upwards for $\psi = 4^\circ$ and with $\psi = 32^\circ$ it is at an angle as indicated. This conforms the experimental and FEM results observed by Vermeer and Sutjiadi [16]. They also state that with an increase in dilatancy angle, the width of the shear band increases, which can also be seen here.

6. CONCLUSIONS AND DISCUSSIONS

The formulation of the MPM discrete governing equations is given. MPM is classified as a so-called point-based or meshless method and is able to model problems where large displacements, deformations and contacts are present.

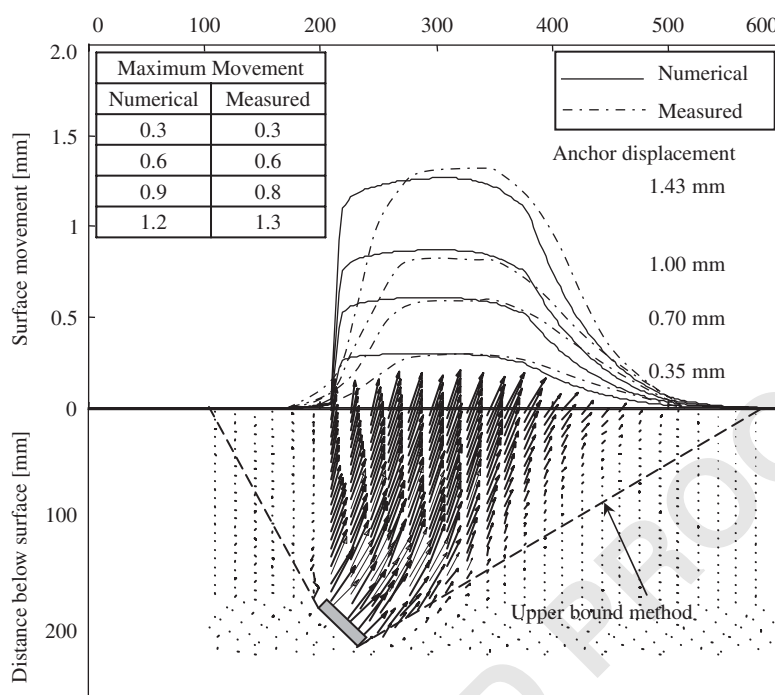


Figure 10. Experimental and predicted movement of the sand.

The results show that MPM can model anchor pull out tests which is difficult to model with FEM. Special FEM contact elements would be needed to model the interface between the soil and the anchor which should be able to model break-away of the soil behind the anchor. The MPM contact model automatically allows break-away since contact correction is only applied at nodes where the two bodies approach each other in the contact normal direction. The bodies are allowed to freely move away from one another.

The ultimate capacity on the vertically pulled anchor was accurately predicted within 5%. It was also shown that the anchor roughness has little effect on the load–displacement curve and on the ultimate capacity. A Mohr–Coulomb constitutive model was used in all the simulations, but it was also shown that the use of a Drucker–Prager model results in a more gradual transition between the elastic and plastic states of the load–displacement curve. Using the two different constitutive models, however, had no significant effect on the ultimate capacity.

The ultimate capacity of the anchor pulled at 45° was accurately predicted within 10%. The predicted movement of the surface corresponded good with measurements.

Convergence with mesh refinement was demonstrated. It was also shown that the width of the shear band decreases with mesh refinement. In the case of the vertically loaded anchor, the angle of the shear band with the vertical was shown to be equal to the dilatancy angle. This phenomenon agrees with results from literature.

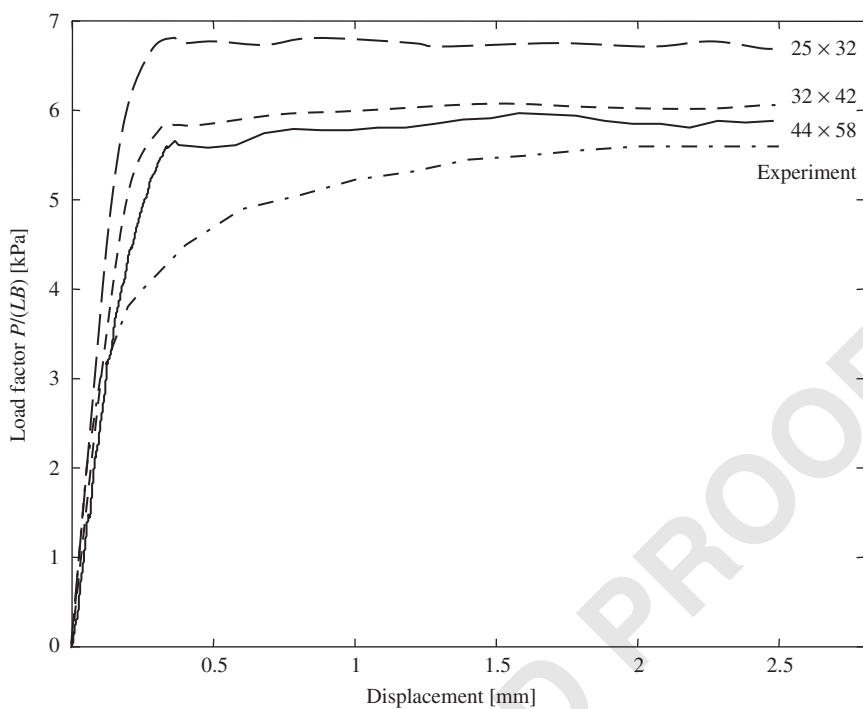


Figure 11. Load–displacement curve for vertically pulled anchor using three mesh sizes, $h/B = 3$.

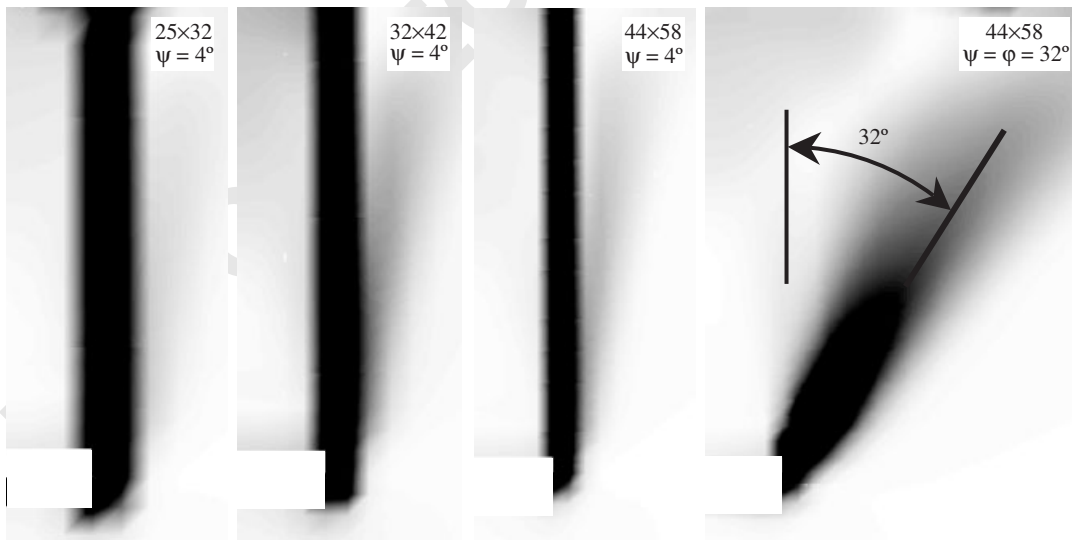


Figure 12. The effect of mesh size and dilatancy angle ψ on the shear bands.

REFERENCES

1. Wieckowski Z. Analysis of granular flow by the material point method. *European Conference on Computational Mechanics*, Cracow, Poland, June 26–29, 2001.
2. Wieckowski Z. The dynamic analysis of large strain problems by the material point method. In Mang HA, Rammerstorfer FG, Eberhardsteiner J (eds). *5th World Congress on Computational Mechanics WCCM V*, Vienna, Austria, July 7–12, 2002.
3. Harlow FH. The particle-in-cell computing method for fluid dynamics. *Methods for Computational Physics* 1964; **3**:319–343.
4. Burgess D, Sulsky D, Brackbill JU. Mass matrix formulation of the FLIP particle-in-cell method. *Journal of Computational Physics* 1992; **103**:1–15.
5. Sulsky D, Chen Z, Schreyer HL. A particle method for history-dependent materials. *Computer Methods in Applied Mechanics and Engineering* 1994; **118**:179–196.
6. Sulsky D, Zhou SJ, Schreyer HL. Application of a particle-in-cell method to solid mechanics. *Computer Physics Communications* 1995; **87**:236–252.
7. Sulsky D, Schreyer HL. Axisymmetric form of the material point method with application to upsetting and Taylor impact problems. *Computer Methods in Applied Mechanics and Engineering* 1996; **139**:409–429.
8. Sulsky D, Schreyer HL. A particle method with large rotations applied to the penetration of history-dependent materials. *Advances in Numerical Simulation Techniques for Penetration and Perforation of Solids, ASME, AMD* 1993; **171**:95–102.
9. Rowe RK, Davis EH. The behaviour of anchor plates in sand. *Geotechnique* 1982; **32**(1):25–41.
10. Rowe RK, Davis EH. The behaviour of anchor plates in clay. *Geotechnique* 1982; **32**(1):9–23.
11. Hassenpflug WC. Matrix tensor notation. Part I: rectilinear orthogonal coordinates. *Computers and Mathematics with Applications* 1993; **26**(3):55–93.
12. Brackbill JU, Kothe DB, Ruppel HM. A low dissipation particle-in-cell method for fluid flow. *Computational Physics Communications* 1988; **48**:25–38.
13. FLAC, *Fast Lagrangian Analysis of Continua: Theory and Background*, 1998. www.itscag.com.
14. Chen Z, Hu W, Shen L, Xin X, Brannon R. An evaluation of the MPM for simulating dynamic failure with damage diffusion. *Engineering Fracture Mechanics* 2002; **69**:1873–1890.
15. Bardenhagen SG, Brackbill JU, Sulsky DL. The material-point method for granular materials. *Computational Methods in Applied Mechanics and Engineering* 2000; **187**:529–541.
16. Vermeer PA, Sutjiadi W. The uplift resistance of shallow embedded anchors. *Proceedings of the 11th International Conference on Soil Mechanics and Foundation Engineering*, vol. 3. A. A. Balkema: Rotterdam, Boston, 1985; 1635–1638.
17. Murray EJ, Geddes JD. Resistance of passive inclined anchors in cohesionless medium. *Geotechnique* 1989; **39**(3):417–431.
18. Jaky J. The coefficient of earth pressure at rest. *Journal for Society of Hungarian Architects and Engineers* 1944; **October**:355–358.



WILEY

John Wiley & Sons Ltd

The Atrium, Southern Gate, Chichester West, Sussex PO19 8S

Author Queries For NAG 439

While preparing this paper/manuscript for typesetting, the following queries have arisen

Query No	Proof Page / line no	Details required	Authors Response
1		NO QUERIES.	

COPYRIGHT TRANSFER AGREEMENT

Wiley Production No.

Re: Manuscript entitled

(the "Contribution") written by

(the "Contributor") for publication in.....

(the "Journal") published by John Wiley & Sons Ltd ("Wiley").

In order to expedite the publishing process and enable Wiley to disseminate your work to the fullest extent, we need to have this Copyright Transfer Agreement signed and returned to us with the submission of your manuscript. If the Contribution is not accepted for publication this Agreement shall be null and void.

A. COPYRIGHT

1. The Contributor assigns to Wiley, during the full term of copyright and any extensions or renewals of that term, all copyright in and to the Contribution, including but not limited to the right to publish, republish, transmit, sell, distribute and otherwise use the Contribution and the material contained therein in electronic and print editions of the Journal and in derivative works throughout the world, in all languages and in all media of expression now known or later developed, and to license or permit others to do so.
2. Reproduction, posting, transmission or other distribution or use of the Contribution or any material contained therein, in any medium as permitted hereunder, requires a citation to the Journal and an appropriate credit to Wiley as Publisher, suitable in form and content as follows: (Title of Article, Author, Journal Title and Volume/Issue Copyright © [year] John Wiley & Sons Ltd or copyright owner as specified in the Journal.)

B. RETAINED RIGHTS

Notwithstanding the above, the Contributor or, if applicable, the Contributor's Employer, retains all proprietary rights other than copyright, such as patent rights, in any process, procedure or article of manufacture described in the Contribution, and the right to make oral presentations of material from the Contribution.

C. OTHER RIGHTS OF CONTRIBUTOR

Wiley grants back to the Contributor the following:

1. The right to share with colleagues print or electronic "preprints" of the unpublished Contribution, in form and content as accepted by Wiley for publication in the Journal. Such preprints may be posted as electronic files on the Contributor's own website for personal or professional use, or on the Contributor's internal university or corporate networks/intranet, or secure external website at the Contributor's institution, but not for commercial sale or for any systematic external distribution by a third party (eg: a listserver or database connected to a public access server). Prior to publication, the Contributor must include the following notice on the preprint: "This is a preprint of an article accepted for publication in [Journal title] Copyright © (year) (copyright owner as specified in the Journal)". After publication of the Contribution by Wiley, the preprint notice should be amended to read as follows: "This is a preprint of an article published in [include the complete citation information for the final version of the Contribution as published in the print edition of the Journal]" and should provide an electronic link to the Journal's WWW site, located at the following Wiley URL: <http://www.interscience.wiley.com/>. The Contributor agrees not to update the preprint or replace it with the published version of the Contribution.
2. The right, without charge, to photocopy or to transmit on-line or to download, print out and distribute to a colleague a copy of the published Contribution in whole or in part, for the Contributor's personal or professional use, for the advancement of scholarly or scientific research or study, or for corporate informational purposes in accordance with paragraph D2 below.
3. The right to republish, without charge, in print format, all or part of the material from the published Contribution in a book written or edited by the Contributor.
4. The right to use selected figures and tables, and selected text (up to 250 words) from the Contribution, for the Contributor's own teaching purposes, or for incorporation within another work by the Contributor that is made part of an edited work published (in print or electronic format) by a third party, or for presentation in electronic format on an internal computer network or external website of the Contributor or the Contributor's employer. The abstract shall not be included as part of such selected text.
5. The right to include the Contribution in a compilation for classroom use (course packs) to be distributed to students at the Contributor's institution free of charge or to be stored in electronic format in datarooms for access by students at the Contributor's institution as part of their course work (sometimes called "electronic reserve rooms") and for in-house training programmes at the Contributor's employer.

D. CONTRIBUTIONS OWNED BY EMPLOYER

1. If the Contribution was written by the Contributor in the course of the Contributor's employment (as a "work-made-for-hire" in the course of employment), the Contribution is owned by the company/employer which must sign this Agreement (in addition to the Contributor's signature), in the space provided below. In such case, the company/employer hereby assigns to Wiley, during the full term of copyright, all copyright in and to the Contribution for the full term of copyright throughout the world as specified in paragraph A above.
2. In addition to the rights specified as retained in paragraph B above and the rights granted back to the Contributor pursuant to paragraph C above, Wiley hereby grants back, without charge, to such company/employer, its subsidiaries and divisions, the right to make copies of and distribute the published Contribution internally in print format or electronically on the Company's internal network. Upon payment of the Publisher's reprint fee, the institution may distribute (but not re-sell) print copies of the published Contribution externally. Although copies so made shall not be available for individual re-sale, they may be included by the company/employer as part of an information package included with software or other products offered for sale or license. Posting of the published Contribution by the institution on a public access website may only be done with Wiley's written permission, and payment of any applicable fee(s).

E. GOVERNMENT CONTRACTS

In the case of a Contribution prepared under US Government contract or grant, the US Government may reproduce, without charge, all or portions of the Contribution and may authorise others to do so, for official US Government purposes only, if the US Government contract or grant so requires. (Government Employees: see note at end.)

F. COPYRIGHT NOTICE

The Contributor and the company/employer agree that any and all copies of the Contribution or any part thereof distributed or posted by them in print or electronic format as permitted herein will include the notice of copyright as stipulated in the Journal and a full citation to the Journal as published by Wiley.

G. CONTRIBUTOR’S REPRESENTATIONS

The Contributor represents that the Contribution is the Contributor’s original work. If the Contribution was prepared jointly, the Contributor agrees to inform the co-Contributors of the terms of this Agreement and to obtain their signature(s) to this Agreement or their written permission to sign on their behalf. The Contribution is submitted only to this Journal and has not been published before, except for “preprints” as permitted above. (If excerpts from copyrighted works owned by third parties are included, the Contributor will obtain written permission from the copyright owners for all uses as set forth in Wiley’s permissions form or in the Journal’s Instructions for Contributors, and show credit to the sources in the Contribution.) The Contributor also warrants that the Contribution contains no libelous or unlawful statements, does not infringe on the right or privacy of others, or contain material or instructions that might cause harm or injury.

Tick one box and fill in the appropriate section before returning the original signed copy to the Publisher

Contributor-owned work

Contributor’s signature Date

Type or print name and title

Co-contributor’s signature Date

Type or print name and title

Attach additional signature page as necessary

Company/Institution-owned work (made-for-hire in the course of employment)

Contributor’s signature Date

Type or print name and title

Company or Institution (Employer-for Hire)

Authorised signature of Employer Date

Type or print name and title

US Government work

Note to US Government Employees

A Contribution prepared by a US federal government employee as part of the employee’s official duties, or which is an official US Government publication is called a “US Government work”, and is in the public domain in the United States. In such case, the employee may cross out paragraph A1 but must sign and return this Agreement. If the Contribution was not prepared as part of the employee’s duties or is not an official US Government publication, it is not a US Government work.

UK Government work (Crown Copyright)

Note to UK Government Employees

The rights in a Contribution by an employee of a UK Government department, agency or other Crown body as part of his/her official duties, or which is an official government publication, belong to the Crown. In such case, the Publisher will forward the relevant form to the Employee for signature.

WILEY AUTHOR DISCOUNT CARD

As a highly valued contributor to Wiley's publications, we would like to show our appreciation to you by offering a **unique 25% discount** off the published price of any of our books*.

To take advantage of this offer, all you need to do is apply for the **Wiley Author Discount Card** by completing the attached form and returning it to us at the following address:

The Database Group
John Wiley & Sons Ltd
The Atrium
Southern Gate
Chichester
West Sussex PO19 8SQ
UK

In the meantime, whenever you order books direct from us, simply quote promotional code **S001W** to take advantage of the 25% discount.

The newest and quickest way to order your books from us is via our new European website at:

<http://www.wileyeurope.com>

Key benefits to using the site and ordering online include:

- Real-time SECURE on-line ordering
- The most up-to-date search functionality to make browsing the catalogue easier
- Dedicated Author resource centre
- E-mail a friend
- Easy to use navigation
- Regular special offers
- Sign up for subject orientated e-mail alerts

So take advantage of this great offer, return your completed form today to receive your discount card.

Yours sincerely,



Verity Leaver
E-marketing and Database Manager

*TERMS AND CONDITIONS

This offer is exclusive to Wiley Authors, Editors, Contributors and Editorial Board Members in acquiring books (excluding encyclopaedias and major reference works) for their personal use. There must be no resale through any channel. The offer is subject to stock availability and cannot be applied retrospectively. This entitlement cannot be used in conjunction with any other special offer. Wiley reserves the right to amend the terms of the offer at any time.

REGISTRATION FORM FOR 25% BOOK DISCOUNT CARD

To enjoy your special discount, tell us your areas of interest and you will receive relevant catalogues or leaflets from which to select your books. Please indicate your specific subject areas below.

<p>Accounting []</p> <ul style="list-style-type: none"> • Public [] • Corporate [] 	<p>Architecture []</p>
<p>Chemistry []</p> <ul style="list-style-type: none"> • Analytical [] • Industrial/Safety [] • Organic [] • Inorganic [] • Polymer [] • Spectroscopy [] 	<p>Business/Management []</p>
<p>Encyclopedia/Reference []</p> <ul style="list-style-type: none"> • Business/Finance [] • Life Sciences [] • Medical Sciences [] • Physical Sciences [] • Technology [] 	<p>Computer Science []</p> <ul style="list-style-type: none"> • Database/Data Warehouse [] • Internet Business [] • Networking [] • Programming/Software Development [] • Object Technology []
<p>Earth & Environmental Science []</p>	<p>Engineering []</p> <ul style="list-style-type: none"> • Civil [] • Communications Technology [] • Electronic [] • Environmental [] • Industrial [] • Mechanical []
<p>Hospitality []</p>	<p>Finance/Investing []</p> <ul style="list-style-type: none"> • Economics [] • Institutional [] • Personal Finance []
<p>Genetics []</p> <ul style="list-style-type: none"> • Bioinformatics/Computational Biology [] • Proteomics [] • Genomics [] • Gene Mapping [] • Clinical Genetics [] 	<p>Life Science []</p>
<p>Medical Science []</p> <ul style="list-style-type: none"> • Cardiovascular [] • Diabetes [] • Endocrinology [] • Imaging [] • Obstetrics/Gynaecology [] • Oncology [] • Pharmacology [] • Psychiatry [] 	<p>Landscape Architecture []</p>
<p>Non-Profit []</p>	<p>Mathematics/Statistics []</p>
	<p>Manufacturing []</p>
	<p>Material Science []</p>
	<p>Psychology []</p> <ul style="list-style-type: none"> • Clinical [] • Forensic [] • Social & Personality [] • Health & Sport [] • Cognitive [] • Organizational [] • Developmental and Special Ed [] • Child Welfare [] • Self-Help []
	<p>Physics/Physical Science []</p>

I confirm that I am a Wiley Author/Editor/Contributor/Editorial Board Member of the following publications:

SIGNATURE:

PLEASE COMPLETE THE FOLLOWING DETAILS IN BLOCK CAPITALS:

TITLE AND NAME: (e.g. Mr, Mrs, Dr)

JOB TITLE:

DEPARTMENT:

COMPANY/INSTITUTION:

ADDRESS:

.....

.....

.....

TOWN/CITY:

COUNTY/STATE:

COUNTRY:

POSTCODE/ZIP CODE:

DAYTIME TEL:

FAX:

E-MAIL:

YOUR PERSONAL DATA

We, John Wiley & Sons Ltd, will use the information you have provided to fulfil your request. In addition, we would like to:

1. Use your information to keep you informed by post, e-mail or telephone of titles and offers of interest to you and available from us or other Wiley Group companies worldwide, and may supply your details to members of the Wiley Group for this purpose.
 Please tick the box if you do not wish to receive this information
2. Share your information with other carefully selected companies so that they may contact you by post, fax or e-mail with details of titles and offers that may be of interest to you.
 Please tick the box if you do not wish to receive this information.

If, at any time, you wish to stop receiving information, please contact the Database Group (databasegroup@wiley.co.uk) at John Wiley & Sons Ltd, The Atrium, Southern Gate, Chichester, West Sussex PO19 8SQ, UK.

E-MAIL ALERTING SERVICE

We offer an information service on our product ranges via e-mail. If you do not wish to receive information and offers from John Wiley companies worldwide via e-mail, please tick the box .

This offer is exclusive to Wiley Authors, Editors, Contributors and Editorial Board Members in acquiring books (excluding encyclopaedias and major reference works) for their personal use. There should be no resale through any channel. The offer is subject to stock availability and may not be applied retrospectively. This entitlement cannot be used in conjunction with any other special offer. Wiley reserves the right to vary the terms of the offer at any time.

Ref: S001W